INSTITUTE OF PHYSICS PUBLISHING JOURNAL OF PHYSICS D: APPLIED PHYSICS
J. Phys. D: Appl. Phys. **34** (2001) 2241–2247 PII: S0022-3727(01)21021-3

# Deconvolution problems in x-ray absorption fine structure spectroscopy

**K V Klementev**

Moscow State Engineering Physics Institute, 115409 Kashirskoe shosse 31, Moscow, Russia

Received 17 January 2001, in final form 30 April 2001
Published 17 July 2001
Online at stacks.iop.org/JPhysD/34/2241

**Abstract**
A Bayesian method applied to the deconvolution of x-ray absorption spectra is presented. It is shown that due to the ill-posedness of the deconvolution problem, an infinitely large number of different Bayesian solutions (absorption coefficients) exist. However, each solution is shown to give the same Fourier transform (FT) of extended x-ray absorption fine-structure (EXAFS), in a wide range of real space. Since it is the FT which is used for analysis in most EXAFS applications, instrumental and lifetime broadening can reliably be removed from raw EXAFS spectra. Several approaches for the determination of the optimal Bayesian regularization parameter are proposed. Bayesian deconvolution is compared with deconvolution which uses the FT together with the optimal Wiener filtering. In addition, it is shown that using a corresponding XPS spectrum as a deconvolution kernel, one-electron absorptance can, in principle, be extracted from the total absorptance, which gives the opportunity to use a more simple XAFS theory for analysis of experimental spectra.

## 1. Introduction

The chief goal of extended x-ray absorption fine-structure (EXAFS) spectroscopy is the determination of interatomic distances, rms fluctuations in bond lengths etc. This is solved mainly by means of fitting of parameterized theoretical curves to experimental ones. However, there are obstacles for such a direct comparison: theory limitations and systematic errors. Among the latter are various broadening effects. First of all, (i) the experimental broadening arising from the finite energy selectivity of a monochromator and the finite angular size of the x-ray beam. (ii) Even if the x-ray beam was strictly monochromatic, its absorption by the electrons of a deep atomic level gives rise to photoelectrons with the finite energy dispersion, due to the finite natural width of this level and the finite lifetime of the core hole. (iii) For x-ray energies far above the absorption edge, the photoelectron creation process and the process of its propagation occur at essentially different time intervals. With other words, when just created, the photoelectron 'does not know' where and how it will decay. Therefore, the photoionization from the chosen atomic level and excitation of the remaining system can be considered as independent processes. Hence the total absorption cross section (as a probability density of two independent random processes) is given by the convolution of a one-electron cross section and an excitation spectrum $W(\Delta E)$ which is the probability density of the energy $\Delta E$ capture at the electron–hole pair creation and is the quantity measured by x-ray photoemission spectroscopy (XPS). For light elements, there are examples of such deeply probing (more than 1.3 keV) and lengthy XPS spectra (see figure 1, taken from [1]).

For all three cases, the measured absorption coefficient, $\mu_m$, is given by the convolution:

$$\mu_m(E) = W * \mu \equiv \int W(E - E')\mu(E')\,\mathrm{d}E' \qquad (1)$$

in which the broadening profile $W(\Delta E)$ and the meaning of the function $\mu$ depend on the considered problem. These can be, correspondingly, the x-ray spectral density after monochromatization and the cross section of ideally monochromatic irradiation (more strictly, measured intensities should be deconvolved separately, see below); the core-hole Lorentzian function and the cross section with a stationary initial level (of zero width); the excitation spectrum and a one-electron cross section.

In modern EXAFS spectroscopy, it is common practice to account for the broadening processes (i)–(iii) at the stage of *ab initio* calculations by introducing into the one-electron scattering potential the imaginary correlation part. Usually, the choice of the correlation part is dictated by empiric considerations and can be different for different systems.

  

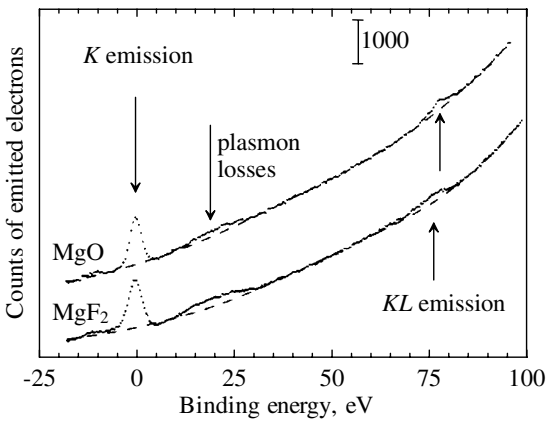


**Figure 1.** XPS spectra of MgO and $MgF_2$ in the vicinity of the Mg 1s peak. Two secondary structures, due to plasmon losses and to double-electron $KL_{2,3}$ excitations, are detected. The energy zero is placed at the Mg $K$ level (∼1300 eV).

Another approach to account for the broadening is to solve the integral in equation (1) for the unknown $\mu$. To find some solution of this equation is not very difficult to do. The simplest way is to use the theorem on the Fourier transform (FT) of convolution, which states that the FT of the convolution integral gives a simple product of the transformed functions. However, the problem of deconvolution is an ill-posed one: it has an unstable solution, or, in other words, it has an infinitely large number of solutions specified by different realizations of noise. Thus, the determination of an optimal, in some sense, solution is required.

A number of papers have addressed the problem of deconvolution, among them those concerning x-ray absorption spectra. Loeffen *et al* [2] applied deconvolution with the Lorentzian function, eliminating the core-hole lifetime broadening. They used a fast FT combined with a Wiener filter. The latter being determined from the noise level which, in turn, is specified by the choice of the limiting FT frequency above which the signal is supposed to be less than the noise. The arbitrariness of such a choice gives rise to rather different deconvolved spectra, which although in [2] was not discussed.

Recently, Filipponi [3] also using the FT for the deconvolution problem with a Lorentzian function, proposed an idea of the decomposition of an experimental spectrum into the sum of a linear contribution, a special analytic function representing the edge, and the oscillating part. For the Lorentzian broadening function, the deconvolution for the first two contributions is found analytically; for the latter one, numerically. The advance of such a decomposition is that, now, the FT of the oscillating part is not dominated by very strong signal of the low-frequency component. Therefore the combination of the forward and backward FTs gives less numerical errors. However, this method is solely suitable for an analytically given broadening function. In addition, in [3] the choice of the filter function (Gaussian) and its parameterization remained vague. Therefore, the issue on the uniqueness or optimality of the found solution was left open.

In the paper by Babanov *et al* [4], a modified Tikhonov regularization method was implemented to the core-hole lifetime deconvolution problem. The idea of the modification was to replace some exact transformation matrix to a well-defined matrix with a voluntarily chosen condition number, implicitly specifying the smoothness of solution. The optimality of such a choice was not discussed.

In all three papers, [2–4], the fact that the core-hole lifetime broadening occurs after the core-hole creation only, i.e. at overcoming the Fermi energy $E_F$, was not taken into account. In those papers, the whole energy range of spectra, including the pre-edge region, was deconvolved with a Lorentzian function.

In early work [5], the statistical approach was proposed for the solution of ill-posed problems. Following that paper, we shall consider in the present paper the deconvolution problem in the framework of the Bayesian method. Its detailed description was given elsewhere [6]. Since the parameterization is naturally involved in the Bayesian method, a principle possibility exists to choose the optimal deconvolution. The problem of such a choice will be scrutinized in this study, which is relevant, by the way, to any spectroscopy. This problem will be shown to be absent for EXAFS spectroscopy because despite the fact that EXAFS spectra themselves do depend on the regularization parameter, their FT does not, in the range of real space used for the analysis. In section 2 we discuss the choice of the optimal deconvolution for a Gaussian model broadening function, in section 3 compare the results of the Bayesian approach with the results of the FT combined with Wiener filtering and, in section 4, we utilize the deconvolution to an experimental spectrum in order to eliminate the aforementioned broadening processes.

## 2. The choice of optimal Bayesian deconvolution

First of all, the deconvolution problem must be shown to have an infinitely large number of solutions. In the present paper, we use as an example the XAFS spectrum of $Nd_{1.85}Ce_{0.15}CuO_{4-\delta}$ at the Cu $K$-edge, collected at 8 K in transmission mode at LURE on beamline D-21. A Si(111) double-crystal monochromator was used, and harmonics were rejected using a plain mirror; the energy step was ∼2 eV, the total amount of points was 826 (from 8850 eV to 10 500 eV), each of them recorded with integration time of 10 s.

Let us take, first, the model broadening function of a simple Gaussian form: $W(E) = C\exp(-E^2/2\Gamma^2)$, where $C$ normalizes $W$ to unity, $\Gamma$ is chosen to be equal to 4 eV. In [6], the method for how to construct a regularized solution of the convolution equation in the framework of the Bayesian approach was described. For that one needs to find eigenvalues and eigenvectors of a special symmetric $(N \times N)$ matrix determined by the experimental spectrum; $N$ is the number of experimental points. Using that approach, let us find a solution, $\mu$, of equation (1) for an arbitrary regularization parameter $\alpha$ and perform then back convolution $W * \mu$, thereby making a solution check. The obtained $\hat{\mu}_m = W * \mu$, ideally, must coincide with $\mu_m$. We introduce the characteristics of the solution quality, given by the normalized difference of these curves:

$$R = \sum_{i=1}^{N}(\mu_{mi} - \hat{\mu}_{mi})^2 \Big/ \sum_{i=1}^{N}\mu_{mi}^2. \qquad (2)$$

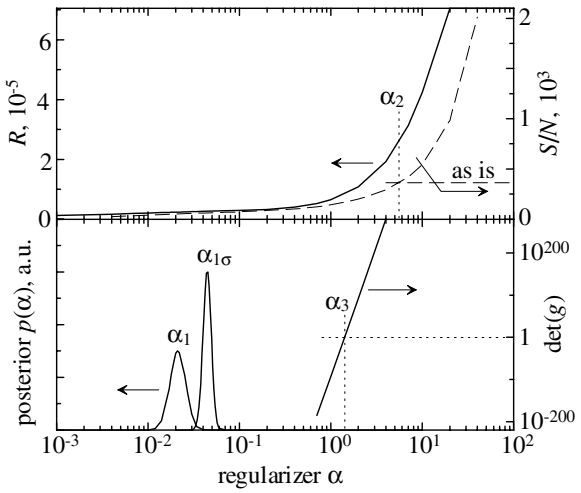


**Figure 2.** (Top) The quality of the deconvolution $R$ against the regularization parameter $\alpha$ (full curve); the dashed curve, denote the lines—signal-to-noise ratio before and after deconvolution. (Bottom) The two peaks denote the posterior density functions $p(\alpha|\boldsymbol{d})$ (left) and $p(\alpha|\boldsymbol{d},\sigma)$ (right) for the regularization parameter $\alpha$. The straight line denotes the determinant of the Bayesian matrix as a function of $\alpha$.

Figure 2 shows the dependence $R$ on $\alpha$. For all $\alpha \lesssim 1$, the quality of the derived solutions is practically the same; denote them as *true* solutions. This fact is a clear manifestation of the ill-posedness of the problem: there is no unique solution. Unfortunately, almost all published works concerning the problem of the deconvolution of XAFS spectra do not disclose this problem. Then, how to chose an optimal solution? It turns out that, for the purposes of EXAFS spectroscopy (and only for EXAFS, not for x-ray absorption near-edge structure (XANES)), there is no need to find an optimal solution and *any* true solution is suitable due for the following observation. Let us find, for any true solution $\mu$, the EXAFS function $\chi(k)\cdot k^w$ in a conventional way, where $k$ is the photoelectron wavenumber, and calculate its FT, $\chi(r)$. In figure 3, we show the EXAFS functions obtained after the Bayesian deconvolution with $\alpha = 1$ and $\alpha = 0.01$, and their corresponding FTs. Despite the fact that the EXAFS spectra themselves do depend on $\alpha$, their FTs practically do not. Thus if one uses $\chi(r)$ for fitting, (in our example, up to $r_{max} = 8$ Å) or a Fourier filtered $\chi(k)$, the search for the optimal $\alpha$ value is no longer relevant.

Nevertheless, below we propose several approaches to the determination of the optimal $\alpha$ value, for instance for XANES spectroscopy needs. The remaining part of this section may be skipped by those readers who are not very familiar with Bayesian methods.

(1) For the regularization parameter $\alpha$ itself, one can introduce the posterior probability density function [5, 6] and choose $\alpha$ with a maximum probability density. This can be done either by using the known standard deviation $\sigma$ of the noise of the absorption coefficient (for our spectrum $\sigma = 9 \times 10^{-4}$, as determined from the FT, following [7]), or by using the most probable value of noise. The definitions of the corresponding conditional probability densities given the data, $p(\alpha|\boldsymbol{d},\sigma)$ and $p(\alpha|\boldsymbol{d})$, can be found elsewhere [6]. For our example spectrum and the chosen model broadening function, these probability densities are drawn in figure 2; their most probable values are found to be $\alpha_{1\sigma} = 0.044$ and $\alpha_1 = 0.021$.

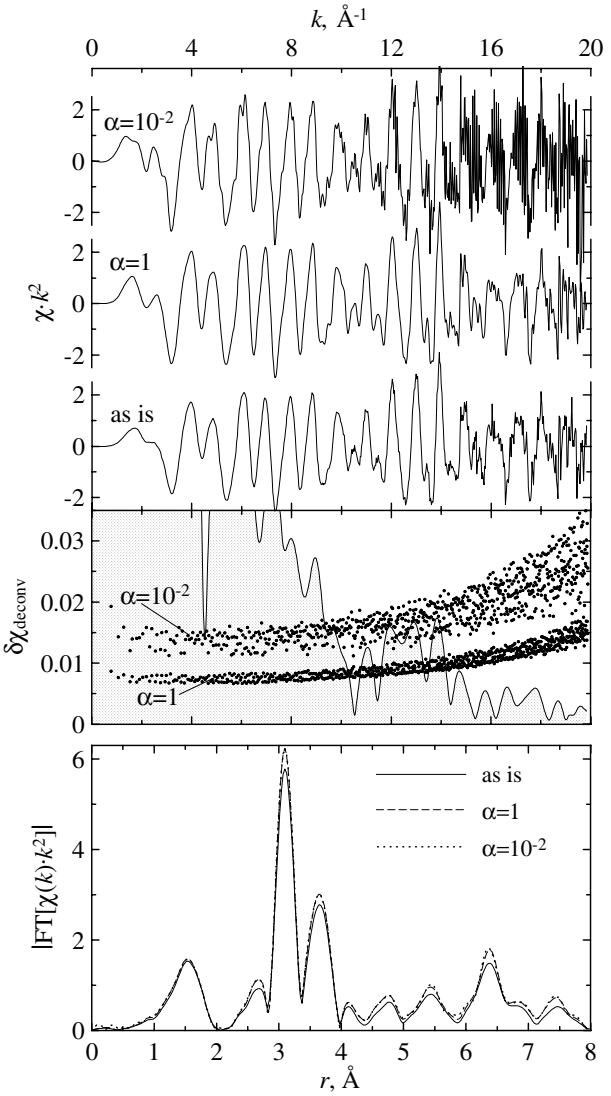


**Figure 3.** (Top) $\chi \cdot k^2$ obtained without deconvolution and after that with $\alpha = 1$ and $\alpha = 0.01$. (Middle) The envelope of the initial $\chi$ (not $k^w$ weighted) and rms deviations of the deconvolved values (dots). (Bottom) The absolute values of the Fourier transform (the dashed and the dotted curves practically merge).

(2) The optimal regularization can be determined from the consideration of the signal-to-noise ratio $S/N$. The Shannon–Hartley theorem states that $I_{max} = B \ln(1 + S/N)$, where $I_{max}$ is the maximum information rate and $B$ is the bandwidth. The authors of [2] suggest that deconvolution is a mathematical operation that conserves information. Therefore, from the theorem it follows that one has to pay for an increase in bandwidth, resulting from deconvolution, via a reduction in the $S/N$ ratio. The hypothesis that $I_{max}$ is conserved is quite questionable, since, for deconvolution, one should introduce *additional* independent information on the profile of broadening. What quantity is conserved in deconvolution is hard to evaluate. In this study, however, for an optimal $\alpha$-value we request the conservation of the $S/N$ ratio. Define $S/N$ as the ratio of mean values of the EXAFS FT spectrum over two regions, $r < 15$ Å and $15$ Å $< r < 25$ Å. The regularization parameter at which the $S/N$ is conserved is denoted in figure 2 as $\alpha_2 = 5.54$. The signal-to-noise

ratio can be defined in a different way. Since the Bayesian methods work in terms of posterior density functions, for each experimental point one can find not only the mean deconvolved value but also the standard deviation $\delta\mu_{deconv}$ [6]. From the latter one finds $\delta\chi = \delta\mu_{deconv}/\mu_0$, where $\mu_0$ is the atomic-like absorption coefficient constructed at the stage of EXAFS function extraction. It is reasonable to compare $\delta\chi$ values with the envelope of the EXAFS spectrum (figure 3, middle). The smaller $\alpha$ is, the more the noise ($\delta\chi$) dominates over the signal (the envelope) in the extended part of the spectrum. The regularization parameter at which the noise and the signal match is the optimal one, $\alpha_2$.

(3) For the Bayesian deconvolution it is necessary to find eigenvalues and eigenvectors of a special symmetric matrix $g$. It turns out that the determinant of this matrix, $\det(g)$, varies with $\alpha$ over hundreds of orders of magnitude. At small $\alpha$'s the matrix is poorly defined, large $\alpha$'s yield very large $\det(g)$ (figure 2). Both cases give large numerical errors because of the ratios of very small or very large values in calculations. As an optimal parameter, we choose $\alpha_3 = 1.41$ at which $\det(g) \sim 1$.

The cases (1) and (2) require one to determine the noise level, which demands additional variables (for instance, the limiting frequencies of FT). Case (3) does not explicitly concern the noise. In addition, because the dependence of $\lg[\det(g)]$ on $\alpha$ appears to be linear, it is easy to find the optimal parameter. Then, case (3) is the most preferred from a practical point of view. Below, for deconvolution of the real broadening processes we use the optimal parameter $\alpha_3$.

## 3. The comparison with Wiener filtering

It is of certain interest to compare the Bayesian method of deconvolution with the widely known method combining optimal Wiener filtering and the convolution theorem. Above we have used the FT, as applied to the EXAFS function $\chi(k) \cdot k^w$, with the conjugate variables $k$ and $2r$ adopted in EXAFS spectroscopy. Now we apply the FT to $\mu_m(E)$ and use the conjugate variables $E$ and $E^{-1}$ (denote as $\tau$). According to the convolution theorem, $\mu_m(\tau) = W(\tau) \cdot \mu(\tau)$, where for a Gaussian broadening function $W(\tau) = \exp(-\Gamma^2\tau^2/2)$. A simple back FT of the ratio $\mu_m(\tau)/W(\tau)$ would give the sought solution $\mu(E)$, but it could be extremely noisy. Therefore, $\mu_m(\tau)$ at large $\tau$ has to be damped. Figure 4 shows the modulus of the FT of the measured spectrum and those of the Bayesian deconvolved spectra with different $\alpha$ values. In the bottom part of figure 4, the corresponding ratios $|\mathrm{FT}\mu|/|\mathrm{FT}\mu_m|$, i.e. the filters transforming $\mu_m(\tau)$ into $\mu(\tau)$, are shown. As seen, the Bayesian deconvolution performs the effective damping of the high-$\tau$ signal, with the limiting frequency $\tau_{max}$ depending on $\alpha$.

The optimal, in the least-squares sense, Wiener filter is expressed as [8]: $\Phi(\tau) = (1 + |n(\tau)|^2/|\mu_m(\tau)|^2)^{-1}$, where $|n(\tau)|^2$ is the power spectrum of the noise replaced here by the mean value of $|\mu(\tau)|^2$ over the range $\tau > 0.4$ eV$^{-1}$, equal to 0.01. As seen in figure 4, the effective Wiener filter $\Phi/W(\tau)$ transforming $\mu_m(\tau)$ to $\mu(\tau)$ is close to the effective filter of the Bayesian deconvolution with $\alpha = 1 \approx \alpha_3$. Thus, the Bayesian deconvolution method and the combined usage of optimal Wiener filtering and the convolution theorem are

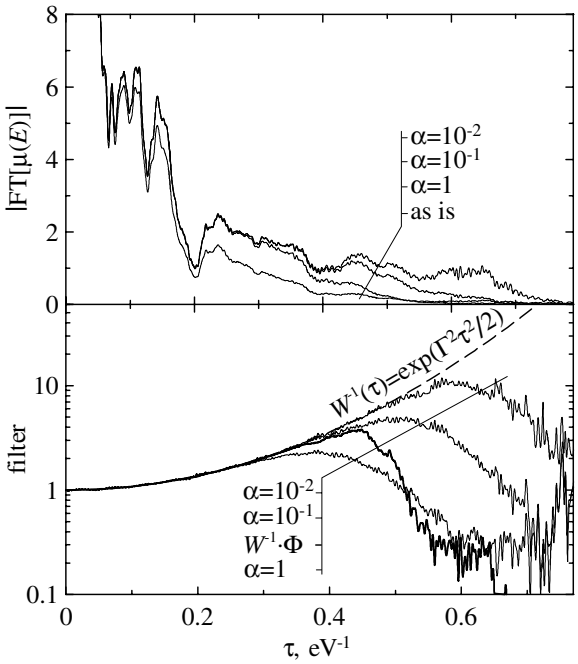


**Figure 4.** (Top) Modulus of the FT of initial $\mu_m$ and deconvolved $\mu$ at different $\alpha$. (Bottom) Filters transforming $\mu_m(\tau)$ into $\mu(\tau)$ obtained after a Bayesian deconvolution (thin full curves), after a deconvolution based on the FT (broken curve) and after a deconvolution based on the combination of the FT and Wiener filtering (thick full curve).

of certain resemblance. Notice, however, that here, for the determination of the Wiener filter, the limiting frequency for the estimation of the noise power spectrum was chosen rather arbitrarily.

As a conclusion of this section, it should be noticed that apart from the possibility of the determination of the deconvolution errors and the possibility of the optimal regularization parameter choice, the Bayesian deconvolution has the advantage to take into account *a priori* information on the smoothness and shape of solution (see details in [6]). In addition, in the Bayesian deconvolution method the broadening function $W(E - E')$ can be of more general form $W(E - E', E)$, i.e. the broadening profile *may change* along the deconvolved curve. This will be very useful in this study: (i) the instrumental broadening is changing along a spectrum because monochromator energy resolution depends noticeably on the angular position and, hence, on the energy of the output x-ray beam; (ii) the lifetime broadening is incipient at $E > E_F$, and the broadening function is a $\delta$-function before $E_F$ and a Lorentzian function after; (iii) the secondary multielectron peaks become non-zero only after overcoming a corresponding excitation energy.

## 4. Applications of deconvolution

We have seen that the Bayesian method proves to be efficient for deconvolution of EXAFS spectra, and the choice of the regularization parameter appears to be irrelevant. Now we perform the deconvolution of various types of broadening. For that we should specify the corresponding broadening functions $W(E - E', E)$.

### 4.1. Instrumental broadening

The monochromator resolution is determined by the rocking curve width $\delta\theta_B$ and by the vertical angular beam size $\delta\theta_\perp$. For the Si(111) flat crystal, the rocking curve width is $\delta\theta_B = 32.4$ $\mu$rad (FWHM) at $E = 9$ keV [9]. The beam divergence (LURE, D-21) $\delta\theta_\perp$ is 150 $\mu$rad. Strictly speaking, the resulting spectral distribution is given by the convolution of the rocking curve and the angular beam profile. But since $\delta\theta_B \ll \delta\theta_\perp$, the energy selectivity is determined by $\delta\theta_\perp$; namely $\delta E/E = \delta\theta_\perp \cot\theta_B = \delta\theta_\perp\sqrt{(2Ed/ch)^2 - 1}$, where $\theta_B$ is the Bragg angle and $d$ is the Bragg plane spacing. Modelling the spectral distribution by a Gaussian function, one obtains:

$$W_{instr}(E - E', E) = C\exp\left[-\frac{(E - E')^2}{2\sigma_\perp^2(E)}\right]$$

$$\sigma_\perp(E) = \frac{\delta E(E)}{2\sqrt{2\ln 2}}$$

where the normalization constant $C$ must be calculated at each $E$ value. For our sample spectrum, $\sigma_\perp(8850\text{ eV}) = 2.46$ eV and $\sigma_\perp(10\,500\text{ eV}) = 3.49$ eV.

### 4.2. Lifetime broadening

At overcoming the absorption edge threshold, the lifetime broadening is described by a Lorentzian function and by a $\delta$-function otherwise:

$$W_{lifetime}(E - E', E) = \begin{cases} \Gamma_K\pi^{-1}[(E - E')^2 + \Gamma_K^2]^{-1} \\ \qquad \text{for } E \geqslant E_F \\ \delta(E - E') \\ \qquad \text{for } E < E_F \end{cases}$$

where $\Gamma_K = 0.775$ eV is half as many as the width of the Cu $K$-level, 1.55 eV (FWHM) [10].

### 4.3. Multielectron broadening

There are certain difficulties in measuring XPS spectra near (and deeper than) the deepest atomic levels. First, monochromatic x-ray sources of high energy are required. Second, for long enough spectra (~100 eV), a photoelectron analyser with a broad energy window and long integration time is necessary. Unfortunately, in the lack of experimental XPS spectra for cuprates near the Cu 1s level, one can only use a model representation of the broadening function. For that, the estimations of position, height and width of the secondary $KM_{23}$ excitation are taken from [11]: $E_{KM_{23}} - E_K = 85$ eV; $I_{KM_{23}}/I_K = 0.03$; $2\Gamma_{KM_{23}} = 3$ eV. Finally, for the broadening function, one has

$$W_{multi-e}(E - E', E) \propto I_K W_{lifetime}(E - E', E) + \begin{cases} \dfrac{I_{KM_{23}}\Gamma_{KM_{23}}}{(E - E' - E_{KM_{23}})^2 + \Gamma_{KM_{23}}^2} & \text{for } E \geqslant E_{KM_{23}} \\ 0 & \text{for } E < E_{KM_{23}}. \end{cases}$$

Here, we should make an additional remark concerning the instrumental broadening. The measured quantity in a XAFS experiment is not an absorption coefficient itself but the intensities of the x-ray beam before, $I_0$, and after, $I$, the sample, and the absorption coefficient is calculated as $\mu_m = \ln(I_0/I)$. Therefore, the instrumental deconvolution should be applied to the intensities, not to $\mu_m$. However, as $I_0(E)$ is a very slow varying function, the difference between these two differently deconvolved $\mu$'s is small: the normalized difference of the form of equation (2) is less than $2 \times 10^{-6}$. Nevertheless, in this study, the instrumental deconvolution is applied separately to the intensities $I_0$ and $I$, and then the instrumentally deconvolved $\mu_{instr}$ is calculated.

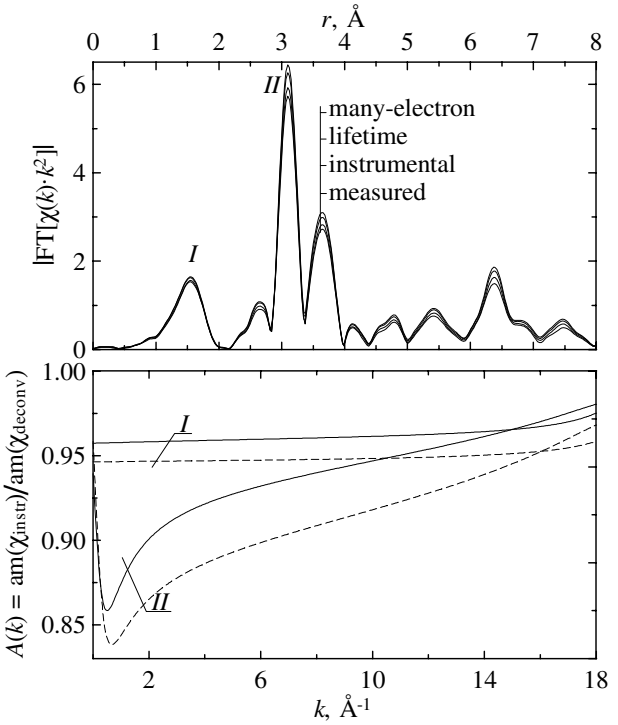


**Figure 5.** (Top) Modulus of the FT of various EXAFS spectra: extracted from the measured absorptance; obtained from the instrumentally deconvolved absorptance, the latter was then deconvolved with the Lorentzian broadening function and with the multielectron broadening function. (Bottom) The path-dependent ratios of amplitudes of initial and deconvolved EXAFS spectra, obtained as a result of the lifetime (full curves) and multielectron (broken curves) deconvolution. First two scattering paths, Cu–O ($I$) and Cu–Nd ($II$), are considered.

Further, having $\mu_{instr}$ as an initial spectrum, the lifetime broadening deconvolution is performed. The multielectron broadening is deconvolved starting also from $\mu_{instr}$. So, the following deconvolutions are carried out: $\mu_m \to \mu_{instr} \rightrightarrows {}^{\mu_{lifetime}}_{\mu_{multi-e}}$.

## 5. Results and discussion

Now, for the deconvolved $\mu$'s, the EXAFS functions are extracted in a conventional way and their FTs are calculated (see figure 5). Just as for the model broadening function in section 2, the deconvolution leads to the increase of the EXAFS magnitude. It turns out that the deconvolution has weak influence on the first FT peak originating from the shortest scattering path. Clearly, the EXAFS oscillations corresponding to this contribution are essentially wider than

the broadening function $W$ (for these, $W$ is 'almost a $\delta$-function', and in equation (1) $\mu$ becomes equal to $\mu_m$). EXAFS oscillations, being of approximately constant period in $k$-space, become quadratically wider in $E$-space in the extended part of a spectrum. Thus, it is in the extended part, where the deconvolved $\mu$ differs less from the initial $\mu_m$. This expectation is met, as illustrated in figure 5 (bottom), where the path-dependent changes in EXAFS amplitude after the lifetime and multielectron deconvolution are drawn.

In modern XAFS theory, various broadening effects are taken into account by introducing the imaginary part to the self-energy [12]. For instance, the lifetime Lorentzian broadening of the EXAFS spectrum with a half-width $\Gamma$ is similar to the effect of the imaginary part of the self-energy with $\mathrm{Im}\,\Sigma = \Gamma$. The experimental broadening is also accounted for by adding an appropriate value to $\mathrm{Im}\,\Sigma$. However, since only transitions to unoccupied levels above $E_F$ are allowed, in *ab initio* calculations, this 'experimental' broadening is incipient only after the edge, despite the fact that real experimental broadening is present along the whole spectrum. Extrinsic losses, which refer to the photoelectron propagation, are also described in terms of the imaginary part of the self-energy operator. Thus, the complexity of the scattering potential is widely used, although it is known that the factorization of $\mu$ into atomic and fine structure parts, $\mu = \mu_0(1+\chi)$, is strictly valid only for real potentials [12, 13].

Intrinsic losses, which refer to excitations in response to creation of the core hole, are usually accounted for by a constant many-body amplitude-reduction factor $S_0^2$, which is either treated as a fitting parameter or estimated from the relaxation of the core hole as the many-electron overlap integral. More precisely, the amplitude reduction is energy and path dependent (as in figure 5), and is given by a convolution-type equation, where the excitation spectrum is represented by a sum of weighted $\delta$-functions [12]. In the present work, the model excitation spectrum and the lifetime broadening are combined together to give the multielectron broadening function. The effect of the introduction of a secondary excitation in addition to the main absorption channel is seen in figure 5. The corresponding overall amplitude reduction is approximately equal to the relative weight of secondary excitations. In addition, there are some phase shifts between the initial spectrum and the deconvolved ones. But these shifts are found to be quite small: less than 0.2 rad at $k < 4$ Å and less than 0.1 rad at $k > 4$ Å.

Being deconvolved with the multielectron broadening function, an EXAFS spectrum should be free from intrinsic losses and should have a zero-width initial level. If one had a real XPS spectrum measured near the Cu 1s level, the XPS spectral features representing the extrinsic losses can also be taken into account via deconvolution. In this case a pure one-electron absorptance could be experimentally obtained, and pure one-electron calculations could be made with real, not complex, scattering potentials. However, there are some reservations on the equivalency of the photoelectron losses in bulk material (as EXAFS sees) and in near-surface layers (as XPS sees). In addition, near the absorption edge, where the photoelectron kinetic energy is low, the core-hole relaxation processes are of certain importance for the photoelectron propagation. Here we do not consider the validity of neglecting this effect (for a review see [12]).

## 6. Conclusions

To take into account the many-electron effects, there exist, in principle, two approaches: (a) to include into a one-electron theory relevant amendments or (b) to extract a one-electron absorptance from the total one, and to use then a pure one-electron theory. The first (and traditional) approach invokes semi-empirical rules (but no *ab initio* calculations) to construct the exchange correlation part of the scattering potential, with the empiricism being based on the comparison with experimental spectra already broadened. In the present paper the principle for the second approach is discussed, using the solution of the integral convolution equation, the kernel in which is the excitation spectrum measured thanks to XPS spectroscopy. Owing to the specific way of the structural information extraction from EXAFS spectra, one uses an isolated signal in $r$-space or a filtered signal in $k$-space. Then there is no violation against the fact that the integral convolution equation is an ill-posed problem, because any one from an infinitely large number of solutions of this equation is appropriate since it gives the same EXAFS FT spectra.

Because of some intrinsic technical difficulties, XPS measurements near deep core levels are challenging. Therefore, the desirable pure one-electron absorptance cannot be experimentally determined at present. Nevertheless, accurate instrumental deconvolution and deconvolution of the lifetime broadening are allowed. These procedures make the comparison between calculated and experimental spectra more immediate and the final results of EXAFS spectroscopy more reliable.

All the stages of EXAFS spectra processing, including those described here, are available in the freeware Windows-based program VIPER [14].

## Acknowledgments

The example spectrum of $Nd_{1.85}Ce_{0.15}CuO_{4-\delta}$ was measured by Professor A P Menushenkov (we thank the LURE staff). The author is indebted to Dr A V Kuznetsov and Dr F Farges for many valuable comments and advice. The work was supported in part by RFBR grant No. 99-02-17343.

## References

[1] Di Cicco A, Crescenzi M D, Bernardini R and Mancini G 1994 *Phys. Rev.* B **49** 2226–9
[2] Loeffen P W, Pettifer R F, Müllender S, van Veenendaal M A, Röler J and Sivia D S 1996 *Phys. Rev.* B **54** 14 877–80
[3] Filipponi A 2000 *J. Phys. B: At. Mol. Opt. Phys.* **33** 2835–46
[4] Babanov Yu A, Ryazhkin A V and Sidorenko A F 1997 *J. Physique IV* **7** Colloq. C2 277–8
[5] Turchin V F, Kozlov V P and Malkevich M S 1971 *Sov. Phys.–Usp.* **13** 681–840
[6] Klementev K V 2001 *J. Phys. D: Appl. Phys.* **34** 209–17
[7] Newville M, Boyanov B I and Sayers D E 1999 *J. Synchrotron Radiat.* **6** 264–5 (Proc. Int. Conf. XAFS X)
[8] Press W H, Teukolsky S A, Vetterling W T and Flannery B P 1992 *Numerical Recipes in Fortran 77: The Art of Scientific Computing* 2nd edn (Cambridge: Cambridge University Press) ch 13.3

[9] Sánchez del Río M, Ferrero C and Mocella V 1997 *Proc. SPIE* **3151** 312–23
[10] Krause M O and Oliver J H 1979 *J. Phys. Chem. Ref. Data* **8** 329–38
[11] Di Cicco A and Sperandini F 1996 *Physica* C **258** 349–59
[12] Rehr J J and Albers R C 2000 *Rev. Mod. Phys.* **72** 621–54
[13] Tyson T A, Hodgson K O, Natoli C R and Benfatto M 1992 *Phys. Rev.* B **46** 5997–6019
[14] Klementev K V 2000 *VIPER for Windows (Visual Processing in EXAFS Researches)* webpage freeware, www.crosswinds.net/∼klmn/viper.html